Therapeutics, Targets, and Chemical Biology

Cancer Research

Preclinical Evaluation of an ^{131}I-Labeled Benzamide for Targeted Radiotherapy of Metastatic Melanoma

John L. Joyal[1], John A. Barrett[1], John C. Marquis[1], Jianqing Chen[1], Shawn M. Hillier[1], Kevin P. Maresca[1], Marie Boyd[2], Kenneth Gage[3], Sridhar Nimmagadda[3], James F. Kronauge[1], Matthias Friebe[4], Ludger Dinkelborg[4], James B. Stubbs[5], Michael G. Stabin[6], Rob Mairs[2], Martin G. Pomper[3], and John W. Babich[1]

Abstract

Radiolabeled benzamides are attractive candidates for targeted radiotherapy of metastatic melanoma as they bind melanin and exhibit high tumor uptake and retention. One such benzamide, *N*-(2-diethylaminoethyl)-4-(4-fluoro-benzamido)-5-iodo-2-methoxy-benzamide (MIP-1145), was evaluated for its ability to distinguish melanin-expressing from amelanotic human melanoma cells, and to specifically localize to melanin-containing tumor xenografts. The binding of [^{131}I]MIP-1145 to melanoma cells *in vitro* was melanin dependent, increased over time, and insensitive to mild acid treatment, indicating that it was retained within cells. Cold carrier MIP-1145 did not reduce the binding, consistent with the high capacity of melanin binding of benzamides. In human melanoma xenografts, [^{131}I]MIP-1145 exhibited diffuse tissue distribution and washout from all tissues except melanin-expressing tumors. Tumor uptake of 8.82% injected dose per gram (ID/g) was seen at 4 hours postinjection and remained at 5.91% ID/g at 24 hours, with tumor/blood ratios of 25.2 and 197, respectively. Single photon emission computed tomography imaging was consistent with tissue distribution results. The administration of [^{131}I]MIP-1145 at 25 MBq or 2.5 GBq/m^2 in single or multiple doses significantly reduced SK-MEL-3 tumor growth, with multiple doses resulting in tumor regression and a durable response for over 125 days. To estimate human dosimetry, gamma camera imaging and pharmacokinetic analysis was performed in cynomolgus monkeys. The melanin-specific binding of [^{131}I]MIP-1145 combined with prolonged tumor retention, the ability to significantly inhibit tumor growth, and acceptable projected human dosimetry suggest that it may be effective as a radiotherapeutic pharmaceutical for treating patients with metastatic malignant melanoma. *Cancer Res; 70(10); 4045–53. ©2010 AACR.*

Introduction

The incidence of malignant melanoma is increasing faster than that of any other cancer in the United States, and The Skin Cancer Foundation estimates that ~60,000 new cases will be diagnosed this year. Unfortunately, the prognosis for stage III and IV disease is poor. Currently, there is no effective treatment for melanoma metastases, and patients with metastatic disease have a life expectancy of 4 to 6 months. Complete surgical removal of the diseased tissue is commonly used to treat the primary tumor. However, due to early and widespread occurrence of metastases as small as 3 mm in diameter, surgery is often not curative, and chemotherapeutic options are limited with poor response rates. Current Food and Drug Administration–approved treatments for stage IV melanoma include dacarbazine, with an objective response rate of 16% (1), and high-dose bolus interleukin 2 (IL-2; proleukin), also with an objective response rate of 16% (2). High-dose interferon α-2b (intron A) is approved for high-risk stage II and III melanoma and has an objective response rate of 14% in stage IV disease (3). The combination of IL-2 and interferon α-2b occasionally produces relatively long durations of response but do not benefit enough patients to improve median survival substantially; in addition, these agents are associated with significant toxicity (4–7). The poor response rates with these regimens suggest a large unmet need for effective treatments for patients with metastatic melanoma.

The vast majority of melanomas contain the pigment melanin (8), which is produced within cells during the metabolism of tyrosine. Melanin is found in all pigmented regions of the body, including the skin, hair, and eyes, and is also found in the inner ear and in regions of the brain, specifically within the substantia nigra (9, 10). Melanins are biopolymers containing indole units with carboxyl functionalities and phenolic hydroxy groups (11), which seem to have multiple homeostatic and protective functions. In the skin, melanin

Authors' Affiliations: [1]Molecular Insight Pharmaceuticals, Cambridge, Massachusetts; [2]University of Glasgow, Glasgow, United Kingdom; [3]Johns Hopkins Medical Institutions, Baltimore, Maryland; [4]Bayer Schering Pharma AG, Global Drug Discovery, Berlin, Germany; [5]Radiation Dosimetry Services, Charlotte, Virginia; and [6]Vanderbilt University, Nashville, Tennessee

Corresponding Author: John W. Babich, Molecular Insight Pharmaceuticals, 160 Second Street, Cambridge, MA 02142. Phone: 617-492-5554; Fax: 617-871-6980; E-mail: jbabich@molecularinsight.com.

doi: 10.1158/0008-5472.CAN-09-4414

protects against the harmful effects of UV radiation, and melanogenesis is stimulated by DNA damage caused by UV rays. In addition, melanin plays a role in absorbing heat. Importantly, organic amines, metals, and polycyclic aromatic hydrocarbons are capable of binding melanin in normal and malignant tissues (12). Drug-melanin associations involve a complex array of hydrogen bonding, hydrophobic and ionic interactions, and both cooperative and anticooperative binding (13, 14). However, those interactions have not been fully characterized, partly because melanins are not well-defined chemical entities but are rather mixtures of polymers with nonhydrolyzable bonds. The physiologic significance of compound binding to normal melanotic tissue is not clear. Although it may lead to the removal of harmful substances from the body (15), it could potentially have detrimental effects as it sequesters toxic or carcinogenic chemicals (9, 12, 14).

Radiolabeled benzamide derivatives are known to bind melanin and exhibit high uptake and retention in melanoma cells and in mice bearing melanoma tumors (16–21), making them potentially effective agents for detecting melanoma in patients and for delivery of therapeutic isotopes. For the last 20 years, efforts have focused on the development of melanin-localizing benzamides that exhibit rapid washout from nontarget tissues and prolonged tumor retention for the treatment of metastatic melanoma. Here, we describe the preclinical evaluation of *N*-(2-diethylamino-ethyl)-4-(4-fluoro-benzamido)-5-iodo-2-methoxy-benzamide (MIP-1145), an ^{131}I-labeled small-molecule benzamide that may be effective for therapeutic targeting of melanin-positive melanoma.

Materials and Methods

Radiolabeling of [^{131}I]MIP-1145 and [^{123}I]MIP-1145. *N*-(2-diethylamino-ethyl)-4-(4-fluoro-benzamido)-2-methoxy-benzamide (MIP-1145 precursor, 80 μg) dissolved in acetic acid was added to thallium trifluoroacetate, $Tl(TFA)_3$, in trifluoroacetic acid (TFA) in a molar ratio of 1:1.2. The solution was brought to a final volume of 0.3 mL (50% acetic acid, 50% TFA). After a 10-minute incubation at room temperature, 2.2 GBq of $Na^{131}I$ [or $Na^{123}I$ for single-photon emission computed tomography (SPECT)/computed tomography (CT)] in 10 to 20 μL of 0.1 N NaOH was added and incubated at room temperature for an additional 5 minutes. The crude reaction was diluted in formulation buffer [6% PEG-400, 2% ethanol, 6% ascorbic acid, and 3% sodium gentisate (pH 4.4)] then purified/analyzed on a Zorbax Eclipse Plus C18, 4.6 × 100 mm, 5 μm reversed phase high performance liquid chromatography (RP-HPLC) column. The column was eluted with a gradient of 25% to 60% buffer B over 10 minutes at a flow rate of 2 mL/min using 2.5% ascorbic acid (w/v)/0.5% acetic acid (v/v) in water (buffer A) and 2.5% ascorbic acid (w/v)/85% ethanol (v/v) in water (buffer B) as solvents. The product peak was collected and diluted in formulation buffer to a final concentration of 1.48 MBq/mL. The solution was filtered through a sterile Millipore Millex GV 33 mm, 0.2 μm syringe filter to yield the final product with a radiochemical purity of >95% and a specific activity as high as 55.5 TBq/mmol.

Cell culture. The human melanoma cell line SK-MEL-3 and the human amelanotic melanoma cell line A375 were obtained from the American Type Culture Collection. A375 cells were maintained in Dulbecco's modified Eagle's medium (DMEM; Invitrogen) supplemented with 10% fetal bovine serum (FBS; Hyclone). SK-MEL-3 cells were maintained in McCoy's 5a (modified) medium (Invitrogen) containing 15% FBS. All cells were grown in a humidified incubator at 37°C/5% CO_2. Cells were passaged by washing in Dulbecco's PBS (D-PBS; Invitrogen) and incubating at 37°C with 0.25% trypsin/EDTA (Invitrogen).

Binding of [^{131}I]MIP-1145 to cells. Cells were plated in Costar 96-well culture plates (50,000 cells per well for SK-MEL-3 and 25,000 cells per well for A375) and allowed to attach overnight. Due to differences in growth rate, plating cells at these densities resulted in both cell lines reaching confluence by the following morning, allowing for a straightforward comparison. To examine the time course of [^{131}I]MIP-1145 uptake, cells were incubated for various times up to 6 hours with 11.5 nmol/L [^{131}I]MIP-1145 (~9×10^5 cpm/well) in DMEM containing 0.5% bovine serum albumin (BSA). At the indicated time, the medium was removed and cells were washed once with DMEM/0.5% BSA. Cells were then washed with a mild acid buffer [50 mmol/L glycine, 150 mmol/L NaCl (pH 3.0)] at 4°C for 5 minutes. The buffer was collected and cells were washed once with DMEM/0.5% BSA. Pooled washes (containing cell surface–bound [^{131}I]MIP-1145) were counted on a Wallac 1282 automated gamma counter. The culture plate (containing cells with internalized [^{131}I]MIP-1145) was counted on a Wallac 1450 Trilux Microbeta liquid scintillation counter. Counts on both instruments were calibrated to a standard. For competitive binding analysis, cells were incubated for 2 hours with 3.6 nmol/L [^{131}I]MIP-1145 in the presence of 1.6 to 1,600 nmol/L nonradiolabeled MIP-1145. All plates were washed twice with DMEM/0.5% BSA containing 50 mmol/L HEPES buffer, 150 μL of scintillation fluid was added per well, and plates were counted on a liquid scintillation counter.

Tissue distribution of [^{131}I]MIP-1145. Male athymic $NCr^{nu/nu}$ mice (Taconic) were anesthetized by an i.p. injection of 9.5 mg/mouse avertin. SK-MEL-3 and A375 cells were resuspended at 8×10^6 cells/mL in a 1:1 mixture of D-PBS containing 1 g/L D-glucose and 36 mg/L L-sodium pyruvate (Invitrogen) and Matrigel (BD Biosciences). Each mouse was injected in the right hind flank with 0.25 mL of the cell suspension. Mice were used for tissue distribution studies when the tumors reached 100 to 500 mm^3 (~21 days postinoculation).

A quantitative analysis of the tissue distribution of [^{131}I]MIP-1145 was done in separate groups of male $NCr^{nu/nu}$ mice bearing SK-MEL-3 or A375 xenografts. [^{131}I]MIP-1145 was administered through the tail vein as a bolus injection of ~74 kBq in a constant volume of 0.05 mL. Mice (n = 5/time point) were euthanized by asphyxiation with carbon dioxide at 1, 4, and 24 hours postinjection. Tissues [blood, heart, lungs, liver, spleen, kidneys, stomach (with contents), large and small

intestines (with contents), testes, skeletal muscle, bone, brain, adipose, and tumor] were dissected, excised, weighed wet, transferred to plastic tubes, and counted in an automated gamma counter.

SPECT imaging. Athymic nude mice were implanted with 5×10^6 SK-MEL-3 or A375 cells. When the tumors reached 100 to 500 mm^3, mice were anesthetized using 1% isoflurane gas in oxygen flowing at 0.6 L/min before and during radiopharmaceutical injection. Mice were injected through the tail vein with 37 MBq [^{123}I]MIP-1145 and imaged at 1, 4, and 24 hours postinjection with a Gamma Medica X-SPECT scanner equipped with two medium-energy collimators with a radius-of-rotation of 9 cm. The tomographic data were acquired in 64 projections over 360° at 40 seconds per projection. Following tomography, CT imaging was acquired in 512 projections to allow anatomic coregistration. Data were reconstructed using the two-dimensional ordered subsets–expectation maximization algorithm. Volume rendered images were generated using Amira 5.2.0 software (Visage Imaging).

Effect of [^{131}I]MIP-1145 on SK-MEL-3 growth. Six-week-old female athymic nude mice (Charles River Laboratories) were inoculated s.c. with human melanoma SK-MEL-3 cells (3×10^6) into the right hind flank. When tumors reached an average volume of ~100 mm^3, animals were randomly assigned to one of the treatment groups (n = 10 mice per group), which included saline, [^{131}I]MIP-1145 at 25 MBq or 2.5 GBq/m^2 single dose, [^{131}I]MIP-1145 once weekly for 2 weeks, and [^{131}I]MIP-1145 once weekly for 3 weeks. Each animal was administered the test article i.p. in a volume of 0.1 mL. Tumor dimensions were measured twice weekly with digital calipers, and tumor volumes were calculated with the formula (width^2 × length)/2. Mice were followed until tumor volumes in the vehicle group reached the maximum allowed by Institutional Animal Care and Use Committee (IACUC) guidelines (1,500 mm^3). To monitor potential toxicity, body weight was measured daily and animals were scored for signs of distress using standard guidelines (22).

Dosimetry in cynomolgus monkeys. Four cynomolgus monkeys (2 females and 2 males) anesthetized with Telazol received an i.v. dose of 185 MBq [^{131}I]MIP-1145 without thyroid blockade. Serial anterior/posterior imaging was performed on a Siemens dual-head E-cam gamma camera. The duration of acquisition was adjusted to achieve adequate organ count density. Blood sampling was performed at 5, 30, 60, 120, and 360 minutes and at 24, 48, and 72 hours postinjection. Urine was collected from all animals through the 72-hour time point at the following collection intervals: 0 to 6, 6 to 24, 24 to 48, and 48 to 72 hours postinjection.

The pharmacokinetics of [^{131}I]MIP-1145 was analyzed by WinNonlin 4.1 (Pharsight). The blood and tissue concentration-time data were computed by a noncompartment method, and pharmacokinetic parameters (maximum concentration, C_{max}; area under curve, AUC; mean residence time, MRT) were generated. Total clearance (CL) was calculated as CL = dose/AUC, and steady-state volume of distribution (V_{ss}) was calculated as V_{ss} = MRT × CL using model 201. Regions of interest were drawn on the anterior and posterior images over the animal's total body, lung, kidney, thyroid, and eye regions at each time point (where these regions were visible). Total organ uptake was normalized to a percentage of the total body dose where the amount of retention at the first image (before voiding) was 100%. Time integrals of whole body and target organ retention were entered into OLINDA/EXM software (23). The adult male human phantom model was used with a 4.8-hour voiding interval for the urinary bladder. The OLINDA/EXM unit density sphere model was used to estimate average dose to the eye.

Results

Radiolabeling of [^{131}I]MIP-1145. The structure of MIP-1145 is shown in Fig. 1. MIP-1145 was readily radiolabeled with ^{131}I or ^{123}I through Tl(TFA)$_3$, starting with the precursor, *N*-(2-diethylamino-ethyl)-4-(4-fluoro-benzamido)-2-methoxy-benzamide. The crude reaction solution was purified by RP-HPLC, and the product was collected in radiolysis-stabilizing medium [6% ascorbic acid and 3% sodium gentisate (pH 4.5)]. Typically, a radiochemical yield of 70% to 90% with a radiochemical purity of >95% for the final product was obtained. [^{131}I]MIP-1145 was stable in both saline and rat plasma (>94%) at 37°C for at least 24 hours.

[^{131}I]MIP-1145 binds specifically to melanotic cells and is internalized. To examine the binding of [^{131}I]MIP-1145 to melanotic SK-MEL-3 cells and amelanotic A375 cells, confluent cultures were incubated with [^{131}I]MIP-1145 for various times up to 6 hours, and washed with either medium or a mild acid solution to remove the compound that is bound to the cell surface. Figure 2A depicts the total binding of [^{131}I]MIP-1145 and the acid-insensitive binding or internalized compound in SK-MEL-3 and A375 cells. Total binding was approximately twice as great for the SK-MEL-3 cells compared with the A375 cells. These results show a time-dependent, acid-insensitive increase in radioactivity associated with the cellular pellet of SK-MEL-3, but not with A375 cells. After 6 hours, approximately 43% of the total MIP-1145 added to the SK-MEL-3 cells were cell associated, whereas only ~13% of MIP-1145 were associated with A375 cells, indicating that MIP-1145 is preferentially retained within the melanin-expressing SK-MEL-3 cells. A competitive binding assay was performed to evaluate the ability of nonradiolabeled MIP-1145 to compete with [^{131}I]MIP-1145 for binding to melanin in SK-MEL-3 and A375 cells. As shown in Fig. 2B,

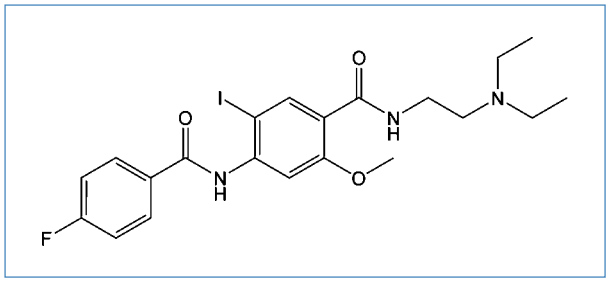

Figure 1. Structure of MIP-1145.

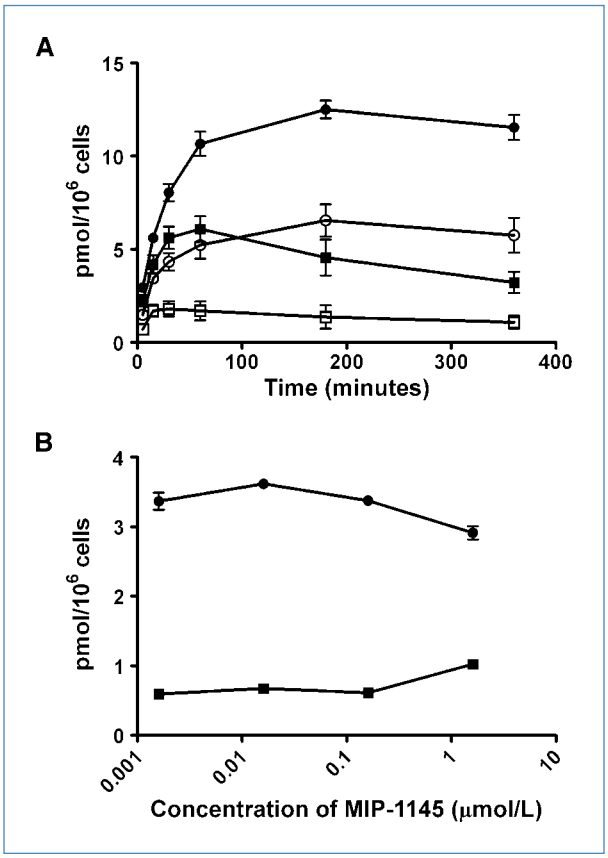

Figure 2. Binding of [^{131}I]MIP-1145 to human melanoma SK-MEL-3 and A375 cells. A, SK-MEL-3 and A375 cells were incubated with 11.5 nmol/L [^{131}I]MIP-1145 for up to 6 hours at 37°C. The medium was removed, and cells were washed with (SK-MEL-3 ○, A375 □) or without (SK-MEL-3 ●, A375 ■) a mild acid solution and counted in a gamma counter. B, SK-MEL-3 (●) and A375 (■) cells were incubated with 3.6 nmol/L [^{131}I]MIP-1145 for 2 hours with increasing amounts of nonradiolabeled MIP-1145.

[^{131}I]MIP-1145 bound to a much greater extent to SK-MEL-3 cells compared with A375 cells. Importantly, there was very little competition by nonradiolabeled MIP-1145 for binding, up to the maximum concentration tested of 1.6 μmol/L. These data suggest a high-capacity binding of MIP-1145 to melanin such that high specific radioactivity is not necessary for effective melanoma uptake.

[^{131}I]MIP-1145 localizes to melanotic tissues. The tissue distribution of [^{131}I]MIP-1145 was assessed in NCr$^{nu/nu}$ mice bearing SK-MEL-3 or A375 xenografts (Table 1). At 1 hour, [^{131}I]MIP-1145 exhibited diffuse tissue distribution with the greatest uptake in the kidneys, gastrointestinal tract, and liver, demonstrating that [^{131}I]MIP-1145 clears through both renal and hepatobiliary routes. By 4 hours, all nontarget and nonexcretory tissues had begun to clear, while uptake in the SK-MEL-3 tumors, but not the A375 tumors, had increased. SK-MEL-3 tumor uptake of 8.82% ID/g was detected at 4 hours postinjection and remained at 5.91% ID/g at 24 hours, with tumor/blood ratios of 25.2 and 197, respectively. Minimal deiodination was observed as the thyroid contained <1% of the total injected dose at all time points. High uptake was noted in the stomach. Although this is unusual, it has been observed with compounds of this class (24). Although we have reported high uptake of [^{131}I]MIP-1145 in the pigmented eyes of C57BL6 mice (>30% ID/g; ref. 25), as expected, there was very little uptake (<1% ID/g) in the unpigmented eyes of the albino NCr$^{nu/nu}$ mice.

SPECT/CT imaging with [^{123}I]MIP-1145 was consistent with the tissue distribution results (Fig. 3). SK-MEL-3 tumors were easily discernible at all time points examined, whereas A375 tumors were not detected. At 1 hour postinjection, diffuse tissue distribution was observed with the greatest uptake in the tumor, kidneys, gastrointestinal tract, and liver. By 24 hours, tumor uptake was still visualized, along with only remnants of [^{123}I]MIP-1145 detected in the lower gastrointestinal tract.

[^{131}I]MIP-1145 inhibits the growth of melanotic xenograft tumors and prolongs survival. To determine if [^{131}I]MIP-1145 has the potential to be used as a radiotherapeutic drug, the effect of [^{131}I]MIP-1145 treatment on tumor growth was examined (Fig. 4A). Twenty-one days after implantation, SK-MEL-3 tumors reached a volume of 123 ± 8 mm^3, and animals were randomly assigned to one of the four treatment groups. Saline treatment resulted in a linear growth rate over the first 60 days of the study. During this time, the tumor size increased >10-fold for a tumor doubling time of approximately 3 days. Several animals in the saline group either died with tumor or had to be sacrificed when the tumor reached the maximum allowed size by IACUC guidelines, 1,500 mm^3. A single dose of [^{131}I]MIP-1145 at 25 MBq or 2.5 GBq/m^2 resulted in a marked reduction in the rate of tumor growth. At 35 days after a single treatment, the average tumor volume was only 2.2 times greater than the starting volume, resulting in a reduction in tumor volume of approximately 79% compared with saline. Two doses of [^{131}I]MIP-1145 administered 1 week apart resulted in tumor regression of 11% at 35 days compared with the starting volume. Three doses of [^{131}I]MIP-1145 administered 1 week apart resulted in a further tumor reduction at 35 days of 40% compared with the starting volume. At 120 days after administration of the first dose of [^{131}I]MIP-1145, inhibition of tumor growth was still obvious in all treatment groups, with the group that received three doses of [^{131}I]MIP-1145 exhibiting no significant tumor growth compared with the initial pretreatment starting volume. [^{131}I]MIP-1145 treatment resulted in a dose-dependent increase in survival. By day 120, 90% of the animals in the saline group either died with tumor or had to be sacrificed (Fig. 4B). In contrast, 60% of the one-dose [^{131}I]MIP-1145 group, 90% of the two-dose [^{131}I]MIP-1145 group, and 100% of the three-dose [^{131}I]MIP-1145 group survived the 120-day course of the experiment. No significant changes in body weight or signs of distress were observed with [^{131}I]MIP-1145 treatment, indicating minimal toxicity.

Dosimetry of [^{131}I]MIP-1145 suggests potential use as a therapeutic in humans. To examine dosimetry, gamma camera imaging and pharmacokinetic analysis was performed on cynomolgus monkeys injected with 185 MBq [^{131}I]MIP-1145. After reaching C_{max} at the first time point,

the blood concentration slowly declined with a MRT of 47 ± 5 hours. Mean blood clearance was 400 ± 45 mL/h, indicating that [^{131}I]MIP-1145 was slowly cleared from the vascular compartment with a V_{ss} of 19 ± 3.1 liters. This value is greater than the total body water of the cynomolgus monkey, indicating that [^{131}I]MIP-1145 was highly distributed outside the vascular compartment. Although this study was not designed to be a mass balance analysis, 28% of the injected dose was recovered in the urine by 72 hours postinjection. Scintigraphic images showed that [^{131}I]MIP-1145 was slowly cleared predominantly through the hepatobiliary route, as evidenced by uptake in the gall bladder and gastrointestinal tract. Ocular retention was observed beginning 24 to 48 hours postinjection. Uptake in the thyroid was also visualized beginning at 24 hours postinjection as expected because thyroid blockade was not conducted.

Radiation dose estimates of [^{131}I]MIP-1145 for human organs were extrapolated from the cynomolgus monkey scintigraphic distribution data. The results of this analysis showed the target organs to be the thyroid, large intestine, and eyes, which received radiation-absorbed doses of 18, 2.8/1.1 (lower/upper), and 1.3 mGy/MBq, respectively. All other organs were predicted to receive between 0.064 and 1.1 mGy/MBq (Table 2).

Discussion

The value of radiolabeled benzamides for imaging melanoma through affinity for melanin was first realized in 1986 when iodine-labeled compounds under investigation for brain imaging were shown to localize to the pigmented eyes of C57BL/6 mice but not the unpigmented eyes of Wistar albino rats (26). It was later determined that uveal melanin mediated the uptake (26). Since these initial observations, several ^{123}I-labeled molecules have been examined for scintigraphic detection of malignant melanoma in patients

Table 1. Tissue distribution of [^{131}I]MIP-1145 in SK-MEL-3 and A375 xenografts (%ID/g, mean ± SD)

	Time (h)		
	1	4	24
SKMEL-3			
Blood	0.75 ± 0.12	0.35 ± 0.04	0.03 ± 0.00
Heart	2.36 ± 0.18	1.32 ± 0.18	0.04 ± 0.03
Lungs	9.70 ± 1.28	6.87 ± 1.33	0.29 ± 0.08
Liver	7.94 ± 1.12	5.18 ± 0.59	0.50 ± 0.07
Spleen	7.26 ± 1.18	3.75 ± 0.60	0.12 ± 0.03
Kidneys	16.55 ± 0.52	13.12 ± 2.68	0.51 ± 0.18
Stomach	12.85 ± 2.53	10.74 ± 2.52	1.41 ± 0.53
Large intestine	2.93 ± 0.54	18.91 ± 3.84	2.24 ± 0.67
Small intestine	15.19 ± 1.50	17.21 ± 2.05	1.03 ± 0.24
Testes	1.51 ± 0.18	1.07 ± 0.09	0.22 ± 0.02
Skeletal muscle	1.39 ± 0.16	0.73 ± 0.16	0.03 ± 0.02
Bone	1.71 ± 0.28	0.95 ± 0.14	0.09 ± 0.08
Brain	0.82 ± 0.06	0.19 ± 0.02	0.01 ± 0.01
Adipose	4.15 ± 2.89	1.03 ± 0.26	0.09 ± 0.05
Tumor	3.77 ± 1.68	8.82 ± 3.55	5.91 ± 3.94
A375			
Blood	0.46 ± 0.05	0.26 ± 0.04	0.04 ± 0.02
Heart	1.96 ± 0.33	1.04 ± 0.06	0.02 ± 0.02
Lungs	9.81 ± 0.88	7.24 ± 1.31	0.37 ± 0.15
Liver	6.79 ± 1.33	4.30 ± 0.45	0.32 ± 0.06
Spleen	4.54 ± 1.34	2.57 ± 0.51	0.15 ± 0.20
Kidneys	14.26 ± 2.73	8.53 ± 1.20	0.21 ± 0.08
Stomach	6.22 ± 2.34	4.57 ± 1.77	0.67 ± 0.27
Large intestine	2.69 ± 0.49	13.81 ± 5.14	1.35 ± 0.36
Small intestine	9.19 ± 3.32	12.44 ± 2.02	0.59 ± 0.24
Testes	1.58 ± 0.22	0.90 ± 0.13	0.16 ± 0.05
Skeletal muscle	1.03 ± 0.09	0.58 ± 0.12	0.02 ± 0.01
Bone	1.34 ± 0.12	0.74 ± 0.07	0.03 ± 0.02
Brain	0.60 ± 0.17	0.16 ± 0.01	0.01 ± 0.00
Adipose	1.56 ± 0.23	1.10 ± 0.46	0.13 ± 0.12
Tumor	2.38 ± 0.75	1.19 ± 0.07	0.04 ± 0.02

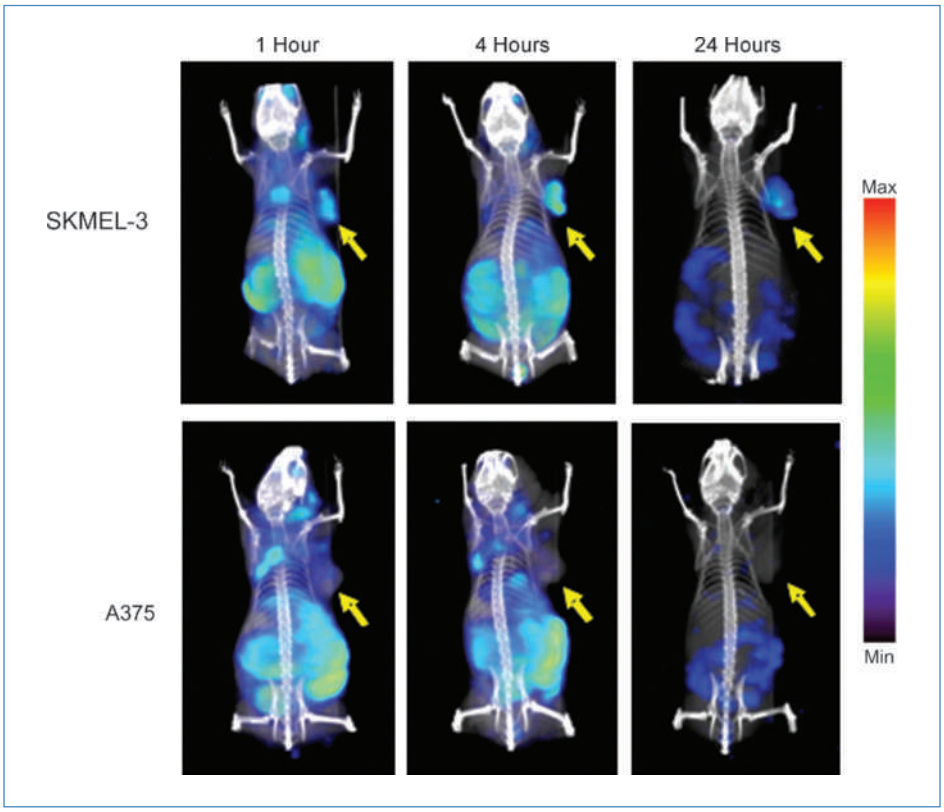

Figure 3. SPECT/CT imaging of [^{123}I]MIP-1145 in nude mice bearing human melanoma SK-MEL-3 and A375 xenografts at 1, 4, and 24 hours postinjection. Arrows indicate tumor.

through melanin content (16, 17, 27). *N*-(2-diethylamino-ethyl 4-iodobenzamide; BZA), the first molecule to advance to clinical trials, showed a sensitivity of 81% and a specificity of 100% on a lesion site basis in patients with confirmed melanoma, thereby validating the concept (28).

More recently, several laboratories have focused on the development of benzamide analogues incorporating ^{131}I for radiotherapy (18). Na^{131}I is commonly used to treat thyroid cancer as it emits a high-energy (606 keV) β particle capable of ablating the cancer and its metastases. For consideration for radiotherapy, compounds must exhibit significant uptake and prolonged tumor retention and rapid washout from nontarget tissues. [^{131}I]MIP-1145 was selected as a lead from a series of ring-substituted benzamides based on the level of tumor uptake *in vivo*, chemical stability, and aqueous solubility (25). MIP-1145 retains a similar pharmacophore to BZA and other melanin-binding benzamides, but is modified to include a methoxy group at the 2-position and an iodine at the 5-position of the central aromatic ring, which was used here for radiolabeling with ^{131}I and ^{123}I in high radiochemical yield and purity. In addition, MIP-1145 contains a fluorobenzoate, which could potentially be radiolabeled with ^{18}F for monitoring the success of radiotherapy by positron emission tomography.

[^{131}I]MIP-1145 exhibited melanin-specific binding, washout from nontarget tissues, and prolonged tumor retention, making it an ideal candidate for systemic radiotherapy. The high uptake of [^{131}I]MIP-1145 is in agreement with observations made using other radiolabeled benzamides (16–21) and is consistent with the binding properties of the melanin polymer, which, unlike a typical receptor-ligand interaction, involves multiple types of associations resulting in the sequestration of large amounts of material in essentially a nonspecific, noncompetitive fashion (19). Similarly, tumor uptake in mice bearing B16F10 xenografts was unchanged by lowering the specific activity of the [^{131}I]MIP-1145 by 1,000-fold from 55.5 TBq/mmol to 55.5 GBq/mmol, 10.17 ± 1.81 versus 9.28 ± 2.24% ID/g, respectively (25).

Treatment of mice bearing melanin-containing SK-MEL-3 tumors with a single dose of [^{131}I]MIP-1145 resulted in a dramatic inhibition of tumor growth, with significant tumor regression at multiple doses. These tumor growth inhibition data with [^{131}I]MIP-1145 are notable as there are presently very few effective treatment options for patients with advanced metastatic melanoma. Future dose optimization studies in humans are necessary to select a regimen that is efficacious while delivering the lowest amount of radiation possible to normal tissues to avoid potential toxicity.

As expected, there was very little uptake of [^{131}I]MIP-1145 in the unpigmented eyes of albino NCr$^{nu/nu}$ mice. However, we previously reported a high uptake of [^{131}I]MIP-1145 in the pigmented eyes of C57BL/6 mice (>30% ID/g; ref. 25). Therefore, it was essential to forecast the exposure to the eyes of melanoma patients. Using a Monte Carlo simulation, the radiation dose estimates to the human eye were obtained from monkey scintigraphic data for ^{131}I accumulated in three

melanin-containing substructures (ciliary body, retina, and choroid). The ocular substructure simulation predicted a radiation-absorbed dose of 0.2 MBq-h/MBq, with the highest radiation-absorbed dose to the ciliary body (6.8 Gy for a 3.7 GBq therapeutic dose). Using the results from external beam data, the $TD_{5/5}$ (5% incidence in 5 years) values for retinopathy and cataract induction are 45 and 10 Gy, respectively (29). Therefore, an administered activity of 20.8 GBq would be needed to reach the retina $TD_{5/5}$ of 45 Gy for retinopathy, and an administered activity of 7.7 GBq would be needed to reach the lens $TD_{5/5}$ of 10 Gy for cataracts. Estimates of the human radiation dose for [^{131}I]MIP-1145, based on an extrapolation of nonhuman primate scintigraphy and dosimetry calculations, support the safe administration of therapeutic doses of up to 16.2 GBq with the anticipated dose-limiting organ being the lower large intestine. Based on the mouse xenograft results, the anticipated efficacious human dose will be 2.5 GBq/m^2 or 4.7 GBq/70 kg patient. At this dose, the radiation-absorbed dose to the lower large intestine will be 13.3 Gy, which is 3.3 times less than the allowable radiation exposure limit of 45 Gy, whereas the dose to the eye is only 6.1 Gy. Based on this profile, we anticipate a sufficient therapeutic index to warrant the study of [^{131}I]MIP-1145 in the treatment of stage III and stage IV melanoma. It may also be advantageous to combine [^{131}I]MIP-1145 with chemotherapeutic drugs or radiation-sensitizing agents, as has been done in animal models with [^{131}I]meta-iodobenzylguanidine, to enhance efficacy at low doses of radiation (30–33).

Table 2. Projected human organ radiation-absorbed dose extrapolated from the cynomolgus monkeys (mGy/MBq, mean ± SD)

Adrenals	8.50E–02 ± 1.80E–02
Brain	7.00E–02 ± 1.50E–02
Breasts	6.40E–02 ± 1.40E–02
Eyes	1.30E+00 ± 6.70E–01
Gallbladder wall	1.20E–01 ± 1.90E–02
Lower large intestine wall	2.80E+00 ± 1.80E–02
Small intestine	3.40E–01 ± 1.80E–02
Stomach wall	9.80E–02 ± 1.80E–02
Upper large intestine wall	1.10E+00 ± 1.50E–02
Heart wall	8.00E–02 ± 1.80E–02
Kidneys	1.10E–01 ± 7.70E–02
Liver	8.60E–02 ± 1.70E–02
Lungs	6.70E–02 ± 2.00E–02
Muscle	8.80E–02 ± 1.60E–02
Ovaries	2.00E–01 ± 1.90E–02
Pancreas	9.20E–02 ± 1.90E–02
Red marrow	8.70E–02 ± 1.40E–02
Osteogenic cells	1.60E–01 ± 3.30E–02
Skin	6.60E–02 ± 1.40E–02
Spleen	8.50E–02 ± 1.80E–02
Testes	8.60E–02 ± 1.60E–02
Thymus	7.80E–02 ± 1.70E–02
Thyroid	1.80E+01 ± 1.30E+01
Urinary bladder wall	6.20E–01 ± 4.10E–02
Uterus	1.50E–01 ± 1.80E–02
Total body	1.00E–01 ± 1.60E–02
Effective dose equivalent	9.20E–01 ± 3.70E–01
Effective dose	1.40E+00 ± 6.30E–01

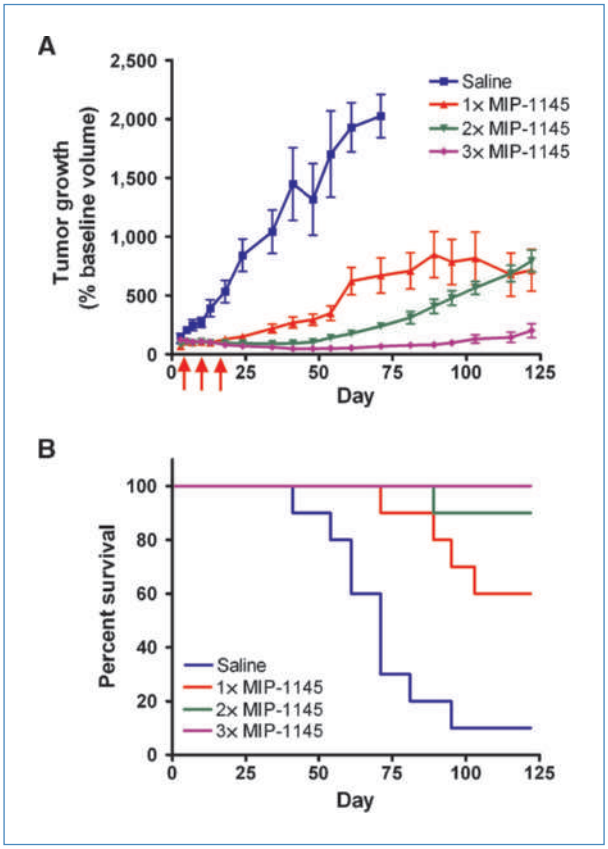

Figure 4. Effect of [^{131}I]MIP-1145 on (A) human melanoma SK-MEL-3 tumor growth and (B) animal survival. [^{131}I]MIP-1145 was administered at 2.5 GBq/m^2 as a single dose, once weekly for 2 weeks, or once weekly for 3 weeks. Arrows indicate treatment days. Tumor growth data are expressed as the percentage change in tumor volume relative to baseline. Survival in each group was calculated as the number of animals that remained in each group at indicated times (animals either died naturally with tumor or were sacrificed when tumors reached 1,500 mm^3).

Although normal melanosomes have a protective function by virtue of their detoxification of reactive oxygen species (ROS), these organelles in melanoma cells are deviant inasmuch as they generate free radicals (34, 35). This may be a result of metal binding to the characteristic pigment structure (36) or a consequence of melanin biosynthesis (37). Chronic production of oxidative stress could contribute to the malignant transformation process (38). Conversely, the melanoma-specific accumulation of ROS may provide a unique therapeutic target (38), and recent evidence indicates that the ROS-inducing drug elesclomol potentiates apoptosis in melanoma cells through the induction of oxidative stress (39). The sensitivity of melanoma cells to therapeutic schemes that promote cell death through ROS production

encourages the use of ionizing radiation combined with the specificity afforded by melanoma-selective targeting using melanin-avid small molecules.

Radiation therapy has not commonly been used to treat melanoma because melanoma cells in culture have traditionally been considered radiation resistant (40). Rofstad, in assessing the effect of radiation on several human melanoma cell lines, concluded that malignant melanoma is heterogeneous in radioresponsiveness, and therefore malignant melanomas should not be considered radiation resistant in general (41, 42). Recently, several clinical studies have realized success using external beam radiation as a means of palliation in patients with metastatic melanoma (43, 44), dispelling the concept that melanoma is radiation resistant. Although focused external radiation may be effective for local control, its use to treat widespread disease is obviously limited. In addition, intense local irradiation can result in significant undesirable damage to adjacent, normal tissues. Targeted radiotherapy, as exemplified here with [^{131}I]MIP-1145, offers the advantage of directing the radioactive payload specifically to tumor cells through binding to a cancer-associated molecular target, thereby sparing nontarget tissues. This should be especially beneficial for patients with widespread metastases where conventional radiotherapy is not applicable.

Interestingly, moderate uptake of [^{131}I]MIP-1145 was detected in the mouse brain, reaching approximately 0.6 to 0.8% ID/g, indicating that [^{131}I]MIP-1145 crosses the blood-brain barrier. Blood-brain barrier permeability is critical for treating melanoma metastases to the brain. This is particularly encouraging given that the presence of brain metastases confers a poor prognosis, and two thirds of melanoma patients die with brain metastases (45).

Alternative strategies to exploit melanin, melanogenesis, and the interaction of benzamides with melanin for the potential treatment of melanoma have met with early, but in some cases limited, success. In this regard, alkylating benzamides have been shown to promote tumor growth delay in preclinical models (46), and high tumor uptake has been observed with radiolabeled acridine-conjugated benzamides (47). Radiolabeled analogues of α-MSH peptide have also shown some promise in animal models (48). Furthermore, radiolabeled antimelanin antibodies for imaging and treatment of melanoma have shown efficacy in preclinical models (49, 50). However, as melanin is intracellular, antibodies are only expected to bind to necrotic tumor cells. In addition, the long circulating half-life of antibodies results in enhanced nontarget tissue exposure, often limiting the dose that can be administered. Thus, small-molecule benzamides, such as [^{131}I]MIP-1145, which freely traverse the cell membrane to reach the intracellular target and clear rapidly from the circulation and nontarget tissues, offer a more effective approach.

In summary, described here is a new radiolabeled benzamide analogue, [^{131}I]MIP-1145, which as a result of its localization to melanin-expressing tumors exhibits efficacy in inhibiting melanoma growth *in vivo*. In light of the large unmet medical need, these data strongly support the advancement of [^{131}I]MIP-1145 to clinical trials for further evaluation as a radiotherapeutic pharmaceutical for treating patients with malignant melanoma.

Disclosure of Potential Conflicts of Interest

J. Joyal, J. Barrett, J. Marquis, J. Chen, S. Hillier, K. Maresca, J. Kronauge, J. Babich, employees, Molecular Insight Pharmaceuticals; R. Mairs, M. Pomper, consultants, Molecular Insight Pharmaceuticals.

Grant Support

NIH and National Cancer Institute grants R44 CA 138041 and U24 CA 92871.

The costs of publication of this article were defrayed in part by the payment of page charges. This article must therefore be hereby marked *advertisement* in accordance with 18 U.S.C. Section 1734 solely to indicate this fact.

Received 12/03/2009; revised 02/23/2010; accepted 03/12/2010; published OnlineFirst 05/04/2010.

References

1. Eggermont AM, Kirkwood JM. Re-evaluating the role of dacarbazine in metastatic melanoma: what have we learned in 30 years? Eur J Cancer 2004;40:1825–36.
2. Atkins MB, Lotze MT, Dutcher JP, et al. High-dose recombinant interleukin 2 therapy for patients with metastatic melanoma: analysis of 270 patients treated between 1985 and 1993. J Clin Oncol 1999;17:2105–16.
3. Sertoli MR, Bernengo MG, Ardizzoni A, et al. Phase II trial of recombinant α-2b interferon in the treatment of metastatic skin melanoma. Oncology 1989;46:96–8.
4. Atallah E, Flaherty L. Treatment of metastatic malignant melanoma. Curr Treat Options Oncol 2005;6:185–93.
5. Tarhini AA, Agarwala SS. Cutaneous melanoma: available therapy for metastatic disease. Dermatol Ther 2006;19:19–25.
6. Tarhini AA, Agarwala SS. Interleukin-2 for the treatment of melanoma. Curr Opin Investig Drugs 2005;6:1234–9.
7. Tarhini AA, Agarwala SS. Novel agents in development for the treatment of melanoma. Expert Opin Investig Drugs 2005;14:885–92.
8. Gualandri L, Betti R, Crosti C. Clinical features of 36 cases of amelanotic melanomas and considerations about the relationship between histologic subtypes and diagnostic delay. J Eur Acad Dermatol 2009;23:283–7.
9. Tolleson WH. Human melanocyte biology, toxicology, and pathology. J Environ Sci Health C 2005;23:105–61.
10. Sulaimon SS, Kitchell BE. The biology of melanocytes. Vet Dermatol 2003;14:57–65.
11. Prota G. Melanins, melanogenesis and melanocytes: looking at their functional significance from the chemist's viewpoint. Pigment Cell Res 2000;13:283–93.
12. Larson BS. Interaction between chemicals and melanin. Pigment Cell Res 1993;6:127–33.
13. Knorle R, Schniz E, Feuerstein TJ. Drug accumulation in melanin: an affinity chromatography study. J Chromatogr B Biomed Sci Appl 1998;714:171–9.
14. Birdelli MG, Ciati A, Crippa PR. Binding of chemicals to melanins re-examined: Adsorption of some drugs to the surface of melanin particles. Biophys Chem 2006;119:137–45.
15. Land EJ, Ramsden CA, Riley PA. Toxicological aspects of melanin and melanogenesis. In: Nordlund JJ, Boissy RE, Hearing VJ, King RA, Oetting WS, Ortonne J, editors. The pigmentary system:

physiology and pathophysiology. 2nd ed. Oxford: Blackwell Publishing Ltd.; 2006.
16. Brandau W, Niehoff T, Pulawski P, et al. Structure distribution relationship of iodine-123-iodobenzamides as tracers for the detection of melanotic melanoma. J Nucl Med 1996;37:1865–71.
17. Larisch R, Schulte K, Vosberg H, et al. Differential accumulation of iodine-123-iodobenzamide in melanotic and amelanotic melanoma metastases *in vivo*. J Nucl Med 1998;39:996–1001.
18. Eisenhut M, Hull WE, Mohammed A, et al. Radioiodinated *N*-(2-diethylaminoethyl)benzamide derivatives with high melanoma uptake: structure-affinity relationships, metabolic fate, and intracellular localization. J Med Chem 2000;43:3913–22.
19. Labarre P, Papon J, Moreau MF, et al. Melanin affinity of *N*-(2-diethylaminoethyl)-4-iodobenzamide, an effective melanoma imaging agent. Melanoma Res 2002;12:115–21.
20. Mansard S, Papon J, Moreau MF, et al. Uptake in melanoma cells of *N*-(2-diethylaminoethyl)-2-iodobenzamide (BZA2), an imaging agent for melanoma staging: relation to pigmentation. Nucl Med Biol 2005; 32:451–8.
21. Pham TQ, Greguric I, Liu X, et al. Synthesis and evaluation of novel radioiodinated benzamides for malignant melanoma. J Med Chem 2007;50:3561–72.
22. Morton DB, Griffiths PHM. Endpoints in animal study protocols. Vet Rec 1985;116:43143.
23. Stabin MG, Sparks RB, Crowe E. OLINDA/EXM: the second-generation personal computer software for internal dose assessment in nuclear medicine. J Nucl Med 2005;46:1023–7.
24. Bonnet-Duquennoy M, Papon J, Mishellany F, et al. Promising pre-clinical validation of targeted radionuclide therapy using a [^{131}I] labeled iodoquinoxaline derivative for an effective melanoma treatment. J Canc Sci Ther 2009;1:1–7.
25. Joyal JL, Hillier SM, Marquis JC, et al. Molecular targeting of melanoma with radiolabeled benzamides. J Nucl Med 2008;49:16P.
26. Michelot JM, Moreau MFC, Labarre PG, et al. Synthesis and evaluation of new iodine-125 radiopharmaceuticals as potential tracers for malignant melanoma. J Nucl Med 1991;32:1573–80.
27. Nicholl C, Mohammed A, Hull WE, Bubeck B, Eisenhut M. Pharmacokinetics of iodine-123-IMBA for melanoma imaging. J Nucl Med 1997;38:127–33.
28. Michelot JM, Moreau MFC, Veyre AJ, et al. Phase II scintigraphic clinical trial of malignant melanoma and metastases with iodine-123-*N*(2-diethylaminoethyl 4-iodobenzamide). J Nucl Med 1993;34: 1260–6.
29. Emami B, Lyman J, Brown A, et al. Tolerance of normal tissue to therapeutic irradiation. Int J Radiat Oncol Biol Phys 1991;21:109–22.
30. McCluskey AG, Boyd M, Gaze MN, Mairs RJ. [^{131}I]MIBG and topotecan: a rationale for combination therapy for neuroblastoma. Cancer Lett 2005;228:221–7.
31. McCluskey AG, Boyd M, Ross SC, et al. [^{131}I]Meta-iodobenzylguanidine and topotecan combination treatment of tumours expressing the noradrenaline transporter. Clin Cancer Res 2005;11:7929–37.
32. Gaze MN, Chang Y-C, Flux GD, Mairs RJ, Saran FH, Meller ST. Feasibility of dosimetry-based high-dose ^{131}I-meta-iodobenzylguanidine with topotecan as a radiosensitiser in children with metastatic neuroblastoma. Cancer Biother Radiopharm 2005;20:195–9.
33. Mairs RJ, Boyd M. Optimizing MIBG therapy of NETs—preclinical evidence of dose maximization and synergy. Nucl Med Biol 2008; 35:S9–20.
34. Gidanian S, Mentelle M, Meyskens FL, Farmer PJ. Melanosomal damage in normal human melanocytes induced by UVB and metal uptake—a basis for the pro-oxidant state of melanoma. Photochem Photobiol 2008;84:556–64.
35. Wittgen HG, van Kempen LC. Reactive oxygen species in melanoma and its therapeutic implications. Melanoma Res 2007;17:400–9.
36. Smit NP, van Nieuwpoort FA, Marrot L, et al. Increased melanogenesis is a risk factor for oxidative DNA damage—study on cultured melanocytes and atypical nevus cells. Photochem Photobiol 2008; 84:550–5.
37. Fruehauf JP, Trapp V. Reactive oxygen species: an Achilles' heel of melanoma? Expert Rev Anticancer 2008;8:1751–7.
38. Fruehauf JP, Meyskens FL. Reactive oxygen species: a breath of life or death? Clin Cancer Res 2007;13:789–94.
39. Kirshner JR, He S, Balasubramanyam V, et al. Elesclomol induces cancer cell apoptosis through oxidative stress. Mol Cancer Ther 2008;7:2319–27.
40. Barranco SC, Romsdahl MM, Humphrey RM. The radiation response of human malignant melanoma cells grown *in vitro*. Cancer Res 1971;31:830–3.
41. Einar R. Radiation sensitivity *in vitro* of primary tumors and metastatic lesions of malignant melanoma. Cancer Res 1992;52:4453–7.
42. Rofstad EK. Radiation biology of malignant melanoma. Acta Radiol Oncol 1986;25:1–10.
43. Olivier KR, Schild SE, Morris CG, Brown PD, Markovic SN. A higher radiotherapy dose is associated with more durable palliation and longer survival in patients with metastatic melanoma. Cancer 2007;110: 1791–5.
44. Berk LB. Radiation therapy as primary and adjuvant treatment for local and regional melanoma. Cancer Control 2008;15:233–8.
45. McWilliams RR, Brown PD, Buckern JC, et al. Treatment of brain metastases from melanoma. Mayo Clin Proc 2003;78:1529–36.
46. Wolf M, Eskerski H, Bauder-Wust U, Haberkorn U, Eisenhut M. Alkylating benzamides with melanoma cytotoxicity: experimental chemotherapy in mouse melanoma model. Melanoma Res 2006; 16:487–96.
47. Desbois N, Gardette M, Papon J, et al. Design, synthesis and preliminary biological evaluation of acridine compounds as potential agents for a combined targeted chemo-radionuclide therapy approach to melanoma. Bioorg Med Chem 2008;16:7671–90.
48. Miao Y, Owen NK, Fischer DR, et al. Therapeutic efficacy of a (188) Re-labeled α-melanocyte-stimulating hormone peptide analog in murine and human melanoma-bearing mouse models. J Nucl Med 2005;46:121–9.
49. Dadachova E, Nosanchuk JD, Shi L, et al. Dead cells in melanoma tumors provide abundant antigen for targeted delivery of ionizing radiation by a mAb to melanin. P Natl Acad Sci U S A 2004;101: 14865–70.
50. Dadachova E, Revskaya E, Sesay MA, et al. Pre-clinical evaluation and efficacy studies of a melanin-binding IgM antibody labeled with (188)Re against experimental human metastatic melanoma in nude mice. Cancer Biol Ther 2008;7:1116–27.